Journal of Cellular Biochemistry 104:2335–2347 (2008)

Fusion Core Structure of the Severe Acute Respiratory Syndrome Coronavirus (SARS-CoV): In Search of Potent SARS-CoV Entry Inhibitors

Ling-Hon Matthew Chu,[1] Siu-Hong Chan,[2] Sau-Na Tsai,[2] Yi Wang,[3] Christopher Hon-Ki Cheng,[4] Kam-Bo Wong,[4] Mary Miu-Yee Waye,[1,4,5] and Sai-Ming Ngai[1,2]*

[1]Molecular Biotechnology Program, The Chinese University of Hong Kong, Hong Kong, China
[2]Department of Biology, The Chinese University of Hong Kong, Hong Kong, China
[3]Department of Cell Biology and Genetics, College of Life Sciences, Peking University, Beijing, China
[4]Department of Biochemistry, The Chinese University of Hong Kong, Hong Kong, China
[5]Department of Biochemistry, Croucher Laboratory for Human Genomics, The Chinese University of Hong Kong, Hong Kong, China

Abstract Severe acute respiratory coronavirus (SARS-CoV) spike (S) glycoprotein fusion core consists of a six-helix bundle with the three C-terminal heptad repeat (HR2) helices packed against a central coiled-coil of the other three N-terminal heptad repeat (HR1) helices. Each of the three peripheral HR2 helices shows prominent contacts with the hydrophobic surface of the central HR1 coiled-coil. The concerted protein–protein interactions among the HR helices are responsible for the fusion event that leads to the release of the SARS-CoV nucleocapsid into the target host-cell. In this investigation, we applied recombinant protein and synthetic peptide-based biophysical assays to characterize the biological activities of the HR helices. In a parallel experiment, we employed a HIV-luc/SARS pseudotyped virus entry inhibition assay to screen for potent inhibitory activities on HR peptides derived from the SARS-CoV S protein HR regions and a series of other small-molecule drugs. Three HR peptides and five small-molecule drugs were identified as potential inhibitors. ADS-J1, which has been used to interfere with the fusogenesis of HIV-1 onto $CD4^+$ cells, demonstrated the highest HIV-luc/SARS pseudotyped virus-entry inhibition activity among the other small-molecule drugs. Molecular modeling analysis suggested that ADS-J1 may bind to the deep pocket of the hydrophobic groove on the surface of the central coiled-coil of SARS-CoV S HR protein and prevent the entrance of the SARS-CoV into the host cells. J. Cell. Biochem. 104: 2335–2347, 2008.

Key words: SARS-CoV; fusion core; peptide

Severe acute respiratory syndrome coronavirus (SARS-CoV) is the causative agent responsible for the worldwide epidemic of respiratory disease and the death of over 800 patients in 2003 [Chim et al., 2003; Ksiazek et al., 2003; Lee et al., 2003]. Intensive researches are underway to search for viral proteins to be used for drug target for anti-SARS therapies in preparation of future recurrences of SARS outbreaks. Amongst different SARS-CoV proteins, the spike (S) protein is of major focus in SARS research for its vital role in target cell recognition and virus entry [Choy et al., 2004; Hofmann and Pohlmann, 2004].

As a type I membrane glycoprotein, S protein is the major component of the characteristic spikes on the surface of SARS-CoV. It contains a total of 1,255 amino acid residues and is the largest structural protein amongst other

Abbreviations used: CD, circular dichroism; HIV-1, human immunodeficiency virus type 1; HR, heptad repeat; HR1, heptad repeat 1; HR2, heptad repeat 2; HR1-DP, deep pocket region of heptad repeat 1; LS, light scattering; MALDI-TOF, Matrix-assisted laser desorption/ionization time-of-flight; MHV, murine hepatitis virus; MW, molecular weight; Native-PAGE, native polyacrylamide gel electrophoresis; S protein, spike glycoprotein; SARS, severe acute respiratory syndrome; SARS-CoV, severe acute respiratory syndrome coronavirus; SEC, size-exclusion chromatography; Tm, transition midpoint temperature.

Grant sponsor: SARS Special RGC; Grant number: CUHK4536/03M; Grant sponsor: Croucher Foundation; Grant sponsor: Special SARS funding from GreaterChina Technology Group Ltd.

*Correspondence to: Sai-Ming Ngai, Department of Biology, The Chinese University of Hong Kong, Shatin, Hong Kong, China. E-mail: smngai@cuhk.edu.hk

Received 17 December 2007; Accepted 24 March 2008
DOI 10.1002/jcb.21790

SARS-CoV proteins. S protein consists of S1 (residues 12–680) and S2 (residues 681–1,255) subunits, respectively [Spiga et al., 2003; Lio and Goldman, 2004]. The S1 subunit of the S protein is responsible for host cell receptor binding and the S2 subunit is responsible for the membrane fusion process. The functional elements of S2 subunit that are involved in SARS-CoV membrane fusion are: a putative fusion peptide (FP) plus two highly conserved 4,3-hydrophobic repeat domains, heptad repeat 1 (HR1) and heptad repeat 2 (HR2). The function of these three sequences had been elucidated in the context of prototypic type I fusion proteins, such as human immunodeficiency virus-1 (HIV-1) gp160 [Eckert and Kim, 2001b]. This suggests a similar membrane fusion mechanism for the SARS-CoV S protein. In HIV-1, binding of S1 subunit to target host cell surface receptor induces global changes in the conformation of S protein, converting the S2 subunit from a native pre-fusion state to a intermediate pre-hairpin state. This receptor-induced conformational change is expected to facilitate the release of the fusion peptide (FP) and position it to interact with the target host cell membrane. The intermediate pre-hairpin then resolves itself into a final fusogenic state [Eckert and Kim, 2001a]. Biophysical studies on SARS-CoV S protein suggests a similar conformational rearrangement, which leads to the association of the two coiled-coil regions within S2 subunit, where three N-terminal HR1 helices interact with three peripheral C-terminal HR2 helices in an anti-parallel manner to form a stable six-helix coiled-coil bundle structure, which is known as SARS-CoV S protein fusion core [Liu et al., 2004; Tripet et al., 2004; Zhu et al., 2004; Xu et al., 2004b]. Such fusion core structure facilitates the juxtaposition of the SARS-CoV onto target cell membranes, destabilizes the membrane lipid bilayers and ultimately causes membrane fusion and the release of SARS-CoV nucleocapsid into the host cell.

The high-resolution structures from X-ray crystallographic analysis of SARS-CoV S protein [Supekar et al., 2004; Xu et al., 2004a; Duquerroy et al., 2005] indicated the presence of the coiled-coil structure in the heptad repeat regions of the S protein fusion core and was confirmed by other biophysical investigations [Liu et al., 2004; Tripet et al., 2004; Zhu et al., 2004; Xu et al., 2004b]. In this study, we have further characterized and confirmed the biologically important interaction of the HR1 and HR2 in the fusion core. The results can facilitate us to investigate the entry inhibitory activities of the HR peptides derived from HR regions and a series of small-molecule drugs that may attenuate the SARS-CoV infection in a pseudotyped virus system. In conclusion, three HR peptides and five small-molecule drugs were identified as potential inhibitors.

RESULTS

Design of Heptad Repeats

By applying the Multicoil program [Wolf et al., 1997] on the S1 polypeptide sequence, we have predicted that the HR1 region of S1 covers 112 amino acid residues (residues 899–1,010). However, it is unlikely that the whole region of HR1 would interact with HR2, which only covers 48 amino acid residues (residues 1,145–1,192).

Two different sites of interactions have been proposed by two individual research teams: (1) Residues 916–950 of HR1 and residues 1,151–1,185 of HR2 [Tripet et al., 2004], and (2) Residues 902–952 of HR1 and residues 1,145–1,184 [Xu et al., 2004b]. In order to clarify the detailed site of interactions between the two heptad repeats, and acquire accurate information for the SARS-CoV S protein fusion core, we have designed synthetic peptides and recombinant proteins that cover both of the HR1 and HR2 regions to study the corresponding protein–protein interactions. Three synthetic peptides were synthesized: HR1-a (residues 899–926), HR1-b (residues 916–950), and HR2 (residues 1,151–1,185), based on the interacting site of HR1 and HR2 suggested by Tripet et al. [2004] (Fig. 1). Three recombinant proteins were designed according to Xu et al. [2004b]: His_6-HR1 (residues 899–958), GST-HR2 or GST-removed-HR2 (residues 1,145–1,192) and HR-2-Helix. HR-2-Helix is an artificial mini coiled-coil where HR1 (899–958) and HR2 (1,145–1,192) are connected by a 10-amino acid linker (GGSGEFGGSG).

HR1 Interacts With HR2 to Form a Six-Helix Bundle of $(HR1)_3$ $(HR2)_3$

Native-polyacrylamide gel electrophoresis (*PAGE*) was used to study the interactions between HR2 and HR1-a/HR1-b peptides. HR2 is negatively charged (pH 6.8) and it enters

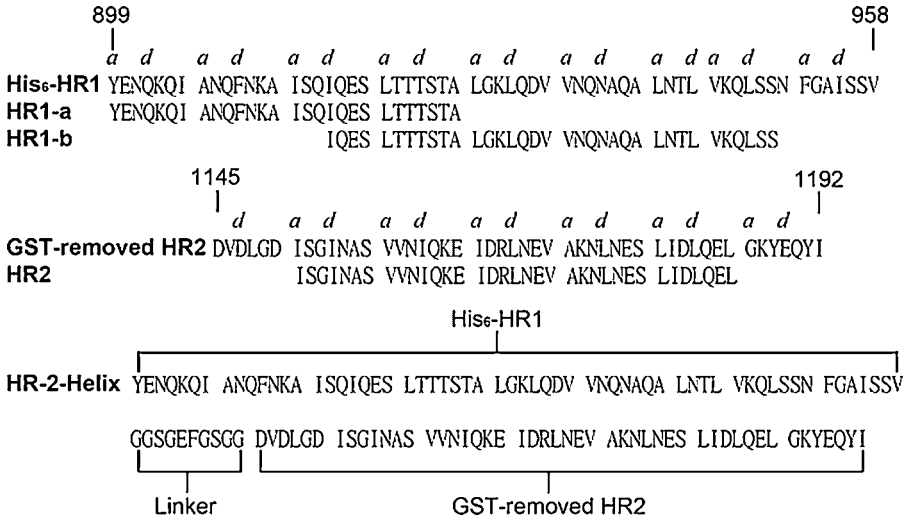

Fig. 1. Amino acid sequences of recombinant proteins and synthetic peptides used in this study. His_6-HR1 (residues 899 iV 958) and GST-removed HR2 (1,145 iV 1,192) are recombinant proteins, whereas HR1-a (residues 899 iV 926), HR1-b (residues 916 iV 950) and HR2 (residues 1,151 iV 1,185) are synthetic peptides. The conserved hydrophobic amino residues, a and d positions of the predicted heptad repeat patterns are shown above the amino acid sequences.

the gel to give a single band (Fig. 2, lane 1). In contrast, HR1-a carries zero charge and HR1-b is positively charged at pH 6.8. Both HR1-a and HR1-b did not enter the gel and could not be visualized upon native gel electrophoresis (lanes 2–5). When HR1-b was pre-incubated with HR2, an extra band of lower mobility was observed. The relative intensity of the resulting protein bands correlated stochiometrically to the molar ratio of HR1-b/HR2 sample mixtures (lanes 6 and 7). No mobility shift of the HR2 band was observed when HR2 was incubated with HR1-a (lanes 8 and 9). The absence of complex formation between HR2 and HR1-a is consistent with the absence of inter-chain interactions between HR2 and the N-terminal region of HR-1 reported previously [Liu et al., 2004; Supekar et al., 2004; Tripet et al., 2004; Xu et al., 2004a,b]. Hence, the C-terminal sequences of HR1 (Ile916-Ser950) contains sufficient determinant for interaction with HR2.

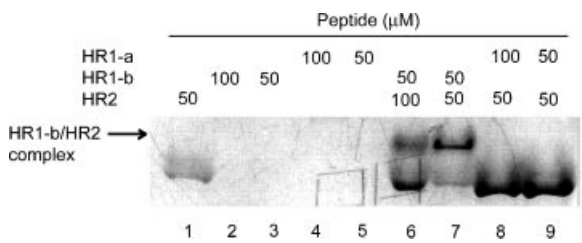

Fig. 2. HR1-b interacts with HR2 in vitro. HR1-a or HR1-b was incubated with HR2 at the indicated concentration before subjected to Native-PAGE analysis. HR1-a and HR1-b are negatively charged in the running pH and do not migrate into the gel on their own (lanes 2–5). A high mobility species was found when HR2 was incubated with HR1-b (lanes 6 and 7) but not with HR1-a (lanes 8 and 9).

Circular dichroism (CD) analysis showed that HR1-b is a random coil, while HR2 peptide displayed a typical CD spectrum for a helical peptide with double minima at 208 and 222 nm. Equal molar mixture of HR1-b/HR2 complex showed enhancement of the total helical content (Fig. 3A), suggesting that the interactions between HR1-b and HR2 promote the helical content of HR-1b. This is consistent with the results reported by Tripet et al. [2004], where enhanced helical content was observed when 50% TFE or equal molar quantity of a peptide equivalent to HR2 was added to a peptide with the same sequence of HR1-b. No significant changes of ellipticity was observed when equal molar HR1-a and HR2 were mixed (result not shown). Thermal denaturation experiments revealed that specific inter-chain interactions were present between HR1-b and HR2. The melting temperature (T_m) of HR2 was 36.3°C (Fig. 3B). When equal molar of HR1-b was added to HR2, the T_m increased by 23.2–59.5°C (Fig. 3C).

Similar to the HR1-b/HR2 interaction, His_6-HR1 and GST-removed-HR2 interacted and acquired enhanced thermostability. His_6-HR1, which spans the combined length of HR1-a and HR1-b, displayed a CD spectrum typical for

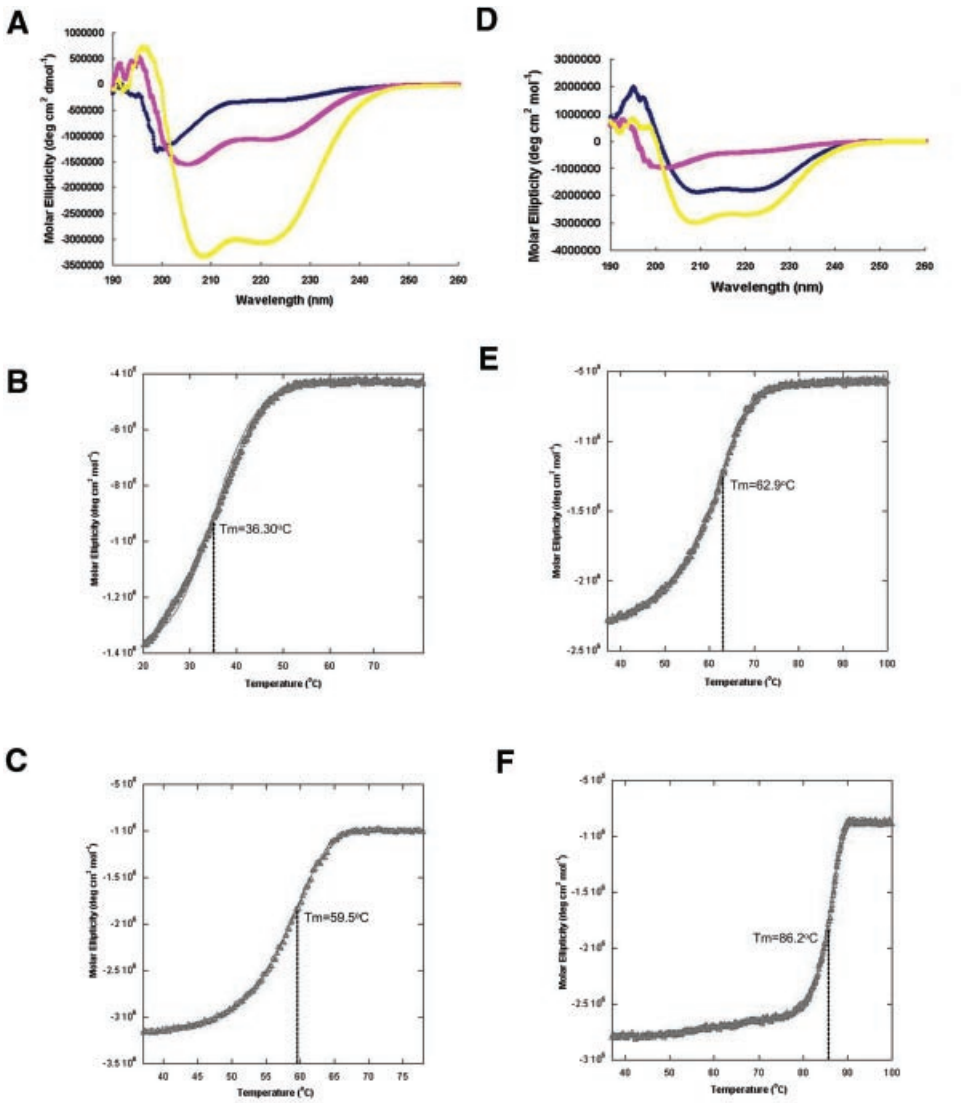

Fig. 3. Folding and thermostability of the peptides and recombinant proteins. **A**: The CD spectra of HR1-b (blue), HR2 (magenta), and HR1-b/HR2 complex (yellow). **B**: Thermal denaturation curve of HR2. The Tm was 36.3°C. **C**: Thermal denaturation curve of HR1-b/HR2 complex. The Tm was 59.5°C. **D**: The CD spectra of His_6-HR1 (blue), GST-removed HR2 (magenta) and the His_6-HR1/GST-removed HR2 complex (yellow). **E**: Thermal denaturation curve of His_6-HR1. The Tm was 62.9°C. **F**: Thermal denaturation curve of His_6-HR1/GST-removed HR2 complex. The Tm was 86.2°C.

helices with double minima at 208 and 222 nm. GST-removed-HR2, however, appeared as a random coil (Fig. 3D). An equal molar mixture of His_6-HR1/GST-removed-eHR2 showed enhancement of the total helical content (Fig. 3D), which reflected interactions between His_6-HR1 and GST-removed-HR2. The interaction also resulted in enhanced thermal stability with an increase of Tm by 23.3°C (from 62.9°C of His_6-HR1 to 89.2°C of the equal molar mixture of His_6-HR1 and GST-removed-HR2; Fig. 3E,F).

Laser light scattering (*LS*) *analysis* was used to study the stoichiometry of HR1, HR2 and their complex. In Figure 4, elution of the proteins was traced by the refractive index of the solution and molar mass distribution plot of relevant peaks was shown on top of the peaks concerned. In each of the traces, the soluble aggregate of the protein loaded was eluted at ~10 ml. On its own, His_6-HR1 (molecular weight of monomer = 9.9 kDa) appeared tetrameric, with a mass of 39 kDa (Fig. 4A), whereas GST-removed-HR2 has a

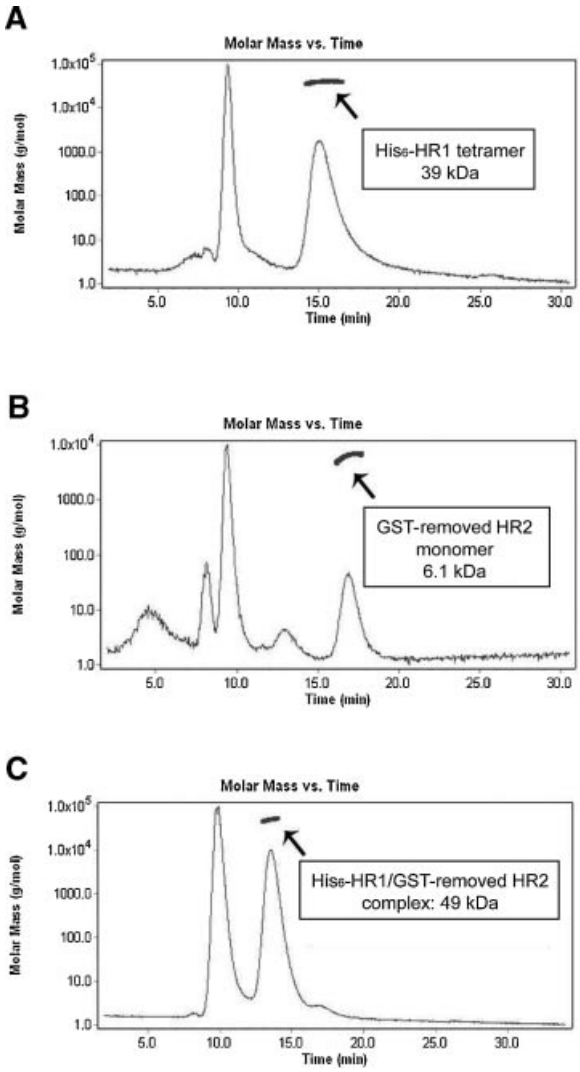

Fig. 4. Laser light scattering analysis of the stoichiometry of the HR1/HR2 complex. Molar mass distribution plots of His_6-HR1 (**A**), GST-removed HR2 (**B**), His_6-HR1/GST-removed HR2 complex (**C**). The solid horizontal bar indicates the average molecular weights for each peak.

mass of 6.1 kDa, suggesting a monomeric form (Fig. 4B). When mixed in equal molar ratio, His_6-HR1/GST-removed-HR2 appeared as a monodispersed species with a molecular weight of 49 kDa (Fig. 4C). This is consistent with a six-helix bundle fusion core conformation with 3 sets of each polypeptides ($3 \times 9{,}910$ (His_6-HR1) $+ 3 \times 6{,}430$ (GST-removed-HR2) $= 49{,}020$ Da) of S proteins [Liu et al., 2004; Supekar et al., 2004; Tripet et al., 2004; Xu et al., 2004a,b].

The mini coiled-coil HR-2-Helix was designed by linking sequences covered by GST-removed-HR2 and HR1 by a 10-amino acid linker (GGSGEFGGSG; Fig. 1). It was characterized using CD spectroscopy and laser LS. The CD profile of HR-2-Helix showed a spectrum typical to helices with double minima at 208 and 222 nm (Fig. 5A). The T_m of HR-2-Helix was 101.00°C (Fig. 5B), indicating strong interactions between the linked HR1 and HR2. HR-2-Helix appeared as a monodispersed peak in LS analysis with an average MW of 40 kDa (Fig. 5C). It is consistent with the expected molecular weight for a trimer of HR-2-Helix ($3 \times 13{,}170.77 = 39{,}512.31$ Da), indicating that the HR-2-Helix self-associated to form a six-helix bundle as reported by Xu et al. [2004a]. These properties suggested that the HR-2-Helix trimeric coiled-coil bundle represents the SARS-CoV S protein fusion core structure of the most stable post-fusion hairpin state.

HIV-luc/SARS Pseudotyped Virus Entry Inhibition Studies

HIV-luc/SARS pseudotyped virus that expressed luciferase and SARS-CoV S protein was constructed and isolated from 293 T cells. Pseudotyped virus entry inhibition assays were done by incubating isolated pseudotyped virus with peptide or small molecule inhibitors before infecting Vero-E6 cells in triplicate (see Experimental Methods Section). Luciferase activity assays were performed on the Vero-E3 cells after overnight incubation with the treated pseudotyped virus.

Peptides HR1-a, HR1-b and HR2, and recombinant protein His_6-HR1 and GST-removed-HR2 were tested for their entry inhibition activity. We found that for the peptide candidates derived from the HR1 region, only HR1-a showed antiviral activity with an EC_{50} of 1.61 μM (Table I). For the peptides derived from the HR2 region, both GST-removed-HR2 and HR2 peptide demonstrated antiviral activities; EC_{50} of GST-removed-HR2 was 2.15 μM, while that of HR2 was 0.34 μM (Table I).

We have also tested the pseudotyped virus entry inhibition activities of 39 small-molecule drugs. Amongst these 39 small-molecule drugs, only 5 of them (Table I) were found to have relatively potent inhibitory activities when compared to quceretin ($EC_{50} = 64.8$ μM): HKC-5 ($EC_{50} = 38.38$ μM), HKC-21 ($EC_{50} = 35.9$ μM), HKC-24 ($EC_{50} = 32.60$ μM), HKC-25 ($EC_{50} = 18.74$ μM) and ADS-J1 ($EC_{50} = 3.89$ μM). Because ADS-J1 showed the highest potency, it was selected for further studies.

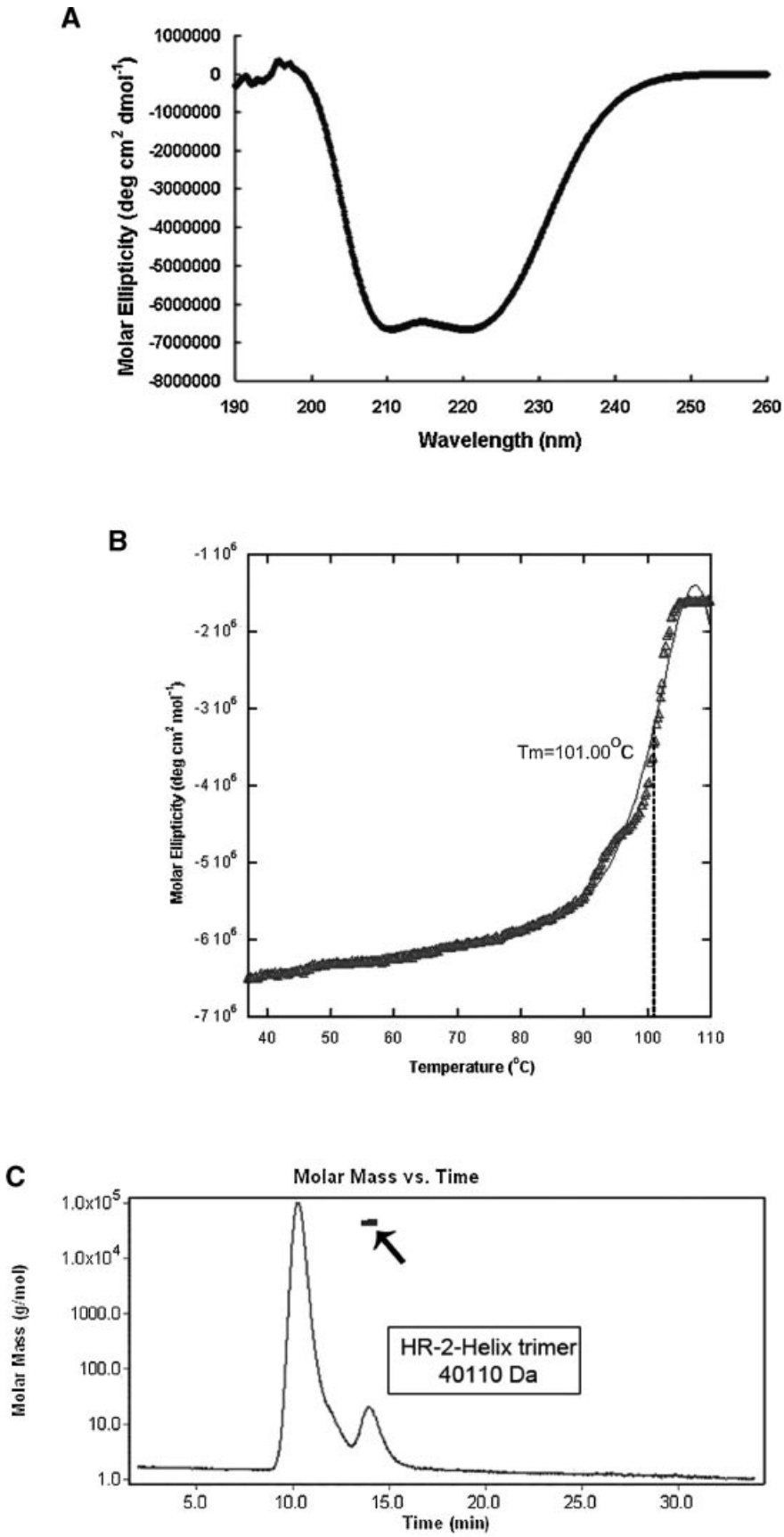

Fig. 5. Characterization of HR-2-Helix. CD spectrum (**A**) and thermal denaturation curve (**B**) are shown. The Tm was 101.00°C. Laser light scattering analysis showed that HR-2-Helix forms a monodispersed species of 40,110 Da. The solid horizontal bar indicates the average molecular weight for the HR-2-Helix peak (**C**).

TABLE I. Viral-Entry Inhibition Activity of Heptad Repeat Peptides and Small Molecules

Peptide	EC_{50} (μM)[a]
His_6-HR1	ND
GST-removed HR2	2.15
HR1-a	1.16
HR1-b	ND
HR2	0.34
Small molecule	**EC_{50} (μM)**
HKC-5	38.38
HKC-21	35.94
HKC-24	32.60
HKC-25	18.74
ADS-J1	3.89
Quercetin	64.80
XXT	ND

ND, not detectable.
[a]All measurements were average values of triplicates.

ADS-J1 Inhibits HR1/HR2 Interactions In Vitro

GST-HR2 and His_6-HR1 were mixed in the presence of ADS-J1, XXT or PBS, followed by immobilization onto glutathione resin. The resin was then washed with PBS and eluted with 10 mM reduced glutathione. The fractions were separated by SDS–PAGE and analyzed by Western blot using anti-His tag antibodies. When incubated with PBS only, majority of His_6-HR1 was detected in the elution fractions (Fig. 6A), showing that His_6-HR1 is bound to GST-HR2. In the presence of ADS-J1, His_6-HR1 was only found in the flow-through but not in the elution fractions (Fig. 6A), whereas XTT had no effect on the interactions and His_6-HR1 was found only in the elution fractions (Fig. 6B). It indicated that ADS-J1 interfered with the interactions between His_6-HR1 and GST-HR2.

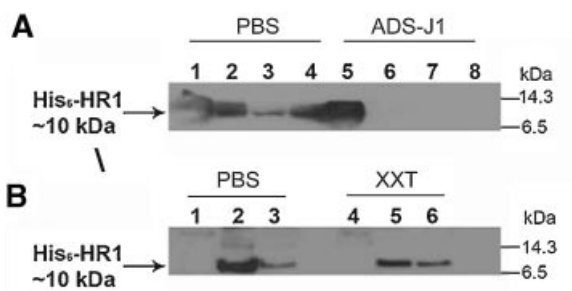

Fig. 6. ADS-J interferes with the interactions between HR1 and HR2 in vitro. His_6-HR1 was preincubated in PBS, control (lanes 1–4, panel A and lanes 1–3, panel B), 1,500 μM ADS-J1 (lanes 5–8, panel A) or 1,500 μM XXT (lanes 4–6, panel B) before loading into the glutathione resin captured GST-HR2. The elution fractions were subjected to SDS–PAGE followed by Western blot analysis probed with anti-His-tag antibodies. Panel A, lanes 1 and 5: flow-through; lanes 2 and 6: first elution; lanes 3 and 7: second elution; lanes 4 and 8: third elution. Panel B, lanes 1 and 4: flow-through; lanes 2 and 5: first elution; lanes 3 and 6: second elution.

In Silico 3D Molecular Modeling

Drug target: The hydrophobic deep pocket in the SARS-CoV S protein fusion core. According to our pseudotyped virus entry inhibition assays, ADS-J1 exhibited the highest entry-inhibition activity. In vitro binding interference assays showed that ADS-J1 interfered with the interactions between HR1 and HR2. From the X-ray crystal structures of the SARS-CoV S protein fusion core, there is a deep pocket located within the relatively deep grooves on the surface of central HR1 coiled-coil (Phe909 to Leu927) [Liu et al., 2004; Supekar et al., 2004; Tripet et al., 2004; Xu et al., 2004a; Duquerroy et al., 2005]. This structural pocket is conserved among heptad repeat region of class I membrane fusion proteins. It has been suggested that the presence of the pocket is important for adapting alternative conformations during fusogenesis [Duquerroy et al., 2005]. Anti-HIV drugs, such as T20, have been developed to target this deep groove [Kilby et al., 1998]. The X-ray crystal structures of SARS-CoV S core peptides showed that four hydrophobic residues from HR2 (Leu1168, Val1171, Leu1175, and Leu1179) penetrate into the deep pocket consisting of Phe909 to Leu920 of HR1 and make extensive hydrophobic contacts with each other (Fig. 7). This region was chosen to be the drug target site for our in silico molecular modeling studies.

Docking of ADS-J1 to the HR1 hydrophobic deep pocket. ADS-J1 was individually positioned in such a way that its hydrophobic groups, phenyl and naphthalene groups, can penetrate into the deep pocket and interact with the hydrophobic residues, Phe909, Ile913, Ile916, and Leu920, within the deep pocket, and with Ala906 outside the pocket. The docking simulations were shown in Figure 7B. Hydrophobic groups of ADS-J1 interact with the hydrophobic residues in the deep pocket and its SO_3H was in close proximity to Lys911 (Fig. 8).

The total docking energy for the simulated complex was monitored accordingly as an indicator of the final ligand placement. The in silico-generated van der Waals energy showed a substantial favorable energy for the complex (-37.05 kcal mol^{-1}), suggesting that

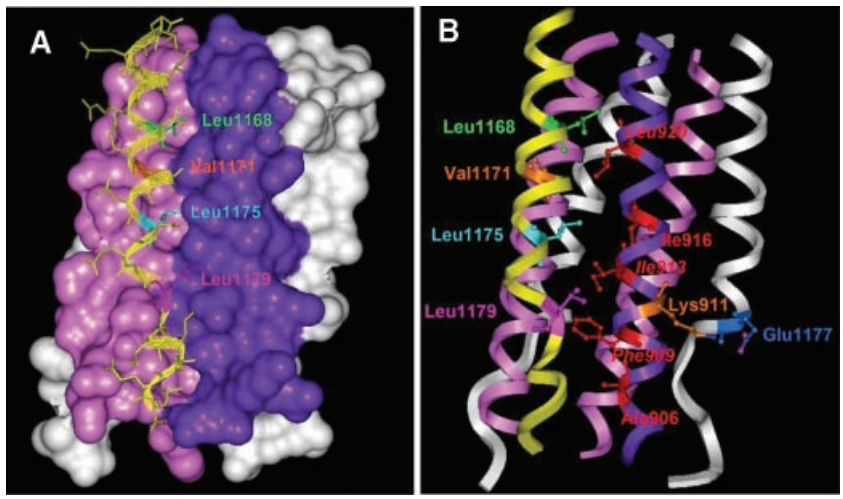

Fig. 7. Interaction of HR2 with the deep pocket in the relative deep groove region of HR1 in the SARS-CoV S protein fusion core. **A**: Hydrophobic residues (Leu1168 (light green), Val1171 (orange), Leu1175 (light blue) and Leu1179 (pink)) of the HR2 helix (yellow) penetrating deep into the deep pocket on the surface of HR1 (violet solid surface). **B**: Interaction of the hydrophobic residues (Phe909, Ile913, Ile916, and Leu920) (red) in the deep pocket formed by the HR1 central coiled-coil (violet ribbon) with the hydrophobic residues of the HR2 helix (yellow ribbon). Note that there is a peripheral ionic HR1/HR2 interaction between Lys911 (orange) on the HR1 helix (violet ribbon) and Glu1177 (blue) on the HR2 helix (white ribbon).

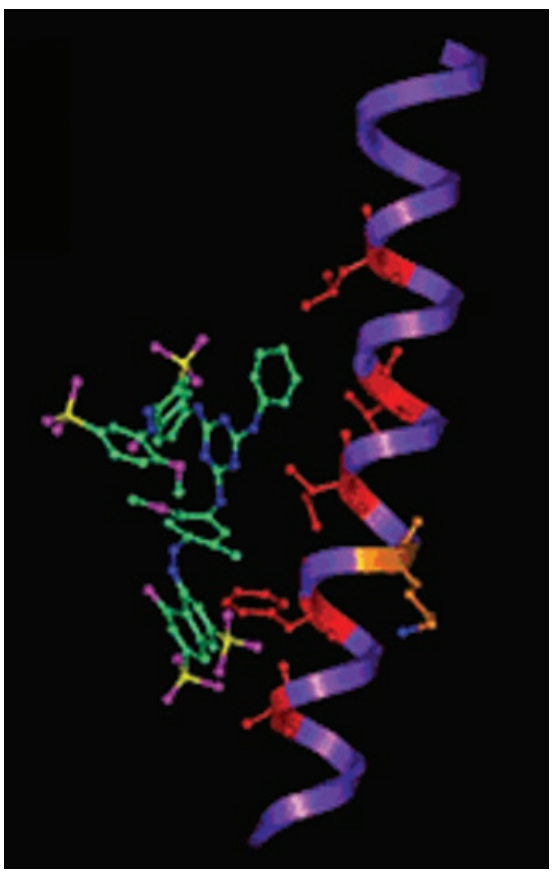

hydrophobic force was the major interactive force between ADS-J1 and the deep pocket of HR1. Such interaction probably hinders the HR1/HR2 interaction in the early stage of SARS-CoV infection. In addition, the small favorable electrostatic energy (-4.41 kcal mol^{-1}) indicated the existence of an ionic interaction. Close visual inspection of the model revealed that the negatively charged sulfonic acid group (SO_3H) of ADS-J1 was in close proximity (8.65 Å) to the positively charged amino side chain of Lys911 outside the deep pocket (Fig. 8).

DISCUSSION

Previous studies of the SARS-CoV S protein fusion core by Tripet et al. [2004] showed that

Fig. 8. Interactions of HR2 and ADS-J1 with the deep pocket of the relatively deep groove region of HR1. The carbon, nitrogen, oxygen, and sulfur atoms of ADS-J1 are shown in green, blue, pink, and yellow, respectively. ADS-J1 was docked onto the deep pocket. The hydrophobic residues in deep pocket of the HR1 helix (violet ribbon) are shown in red and Lys911 is shown in orange with its amino group shown in blue. Hydrophobic interaction between Leu1168 (light green), Val1171 (orange), Leu1175 (light blue) and Leu1179 (pink) of HR2 (yellow ribbon) and the hydrophobic residues (red) in the deep pocket. The molecular weight of ADS-J1 is 1079.01 Da, the calculated energy terms are -37.05 kcal/mol, -4.41 and -41.46 for van der Waals, electrostatic and total energy, respectively. The distance between Lys911 and SO_3H of ADJ-S1 is 8.65 Å.

the site of interaction between HR1 and HR2 consists of HR1 residues 916–950 and HR2 residues 1,151–1,185. However, the six-helix coiled-coil bundle formed by our constructs His_6-HR1 (residues 899–958) and GST-removed-HR2 (residues 1,145–1,192) was shown to be stronger and more stable than that formed by the HR1 (residues 916–950) and HR2 (residues 1,147–1,185) reported by Tripet et al.; the Tm of the complex between His-HR1 and GST-removed-HR2 was 86.2°C compared to 74°C of the HR1/HR2 complex reported by Tripet et al. The major differences between the two constructs are the N-terminal residues 899–916 of HR1 and the C-terminal residues 1,186–1,192 of HR2. Therefore, these two regions are actually important for the interactions between HR1 and HR2 for the formation of a stable fusion core structure.

When the two heptad repeat regions are connected by a flexible linker, a higher thermostability was achieved. The mini-coiled coil HR-2-Helix (consists of the sequence of His-HR1 and GST-removed-HR2 linked by a 10-amino acid linker) has a T_m of 101.0°C, compared to the T_m of 86.2°C of the complex between His-HR1 and GST-removed-HR2. In fact, HR-2-Helix (HR1 residues 899–958 and HR2 residues 1,145–1,192) was even more stable than the mini-coiled coil 2-Helix consisted of HR1 (residues 902–952) and HR2 (residues 1,145–1,184) reported by Xu et al. [2004b]. The T_m of HR-2-Helix in this study was 101.0°C, when compared to 85°C of 2-Helix [Xu et al., 2004b]. The 16°C difference was probably due to the strong hydrophobic and electrostatic interaction between N-terminal HR1 residues 899–916 and C-terminal HR2 residues 1,185–1,192, as discussed earlier, and the shorter linker sequence that allows lower degree of flexibility.

X-ray crystallographic studies of the SARS-CoV S protein fusion core [Liu et al., 2004; Supekar et al., 2004; Tripet et al., 2004; Xu et al., 2004a; Duquerroy et al., 2005] have demonstrated that three HR2 helices pack against the hydrophobic grooves on the surface of the HR1 central coiled-coil trimer and form a six-helix coiled-coil bundle, in which the helical regions of HR2 (residues 1,161–1,175) pack exactly against the relatively deep grooves of HR1 (residues 909–927) and the extended regions of HR2 (residues 1,151–1,160; 1,176–1,185) pack against the relatively shallow grooves (residues 928–952). The structures also showed that the N-terminal HR1 residues 899–916 actually form half of the relatively deep groove region for the binding of the HR2 helical regions and make extensive interactions with residues 1,161–1,192. It has recently been reported that complex of peptides that span residues 926–962 and 1,150–1,183, respectively forms four-helix bundle (dimer of heterodimers) in crystal packing [Deng et al., 2006]. A "wedges-to-grooves" mode of packing was observed within the helix bundle with inter-helical Leu side-chains in van der Waals contact. The Tm of the complex is 64°C. This four-helix bundle state is considered one of the intermediate states of folding/unfolding of the fusion core structure during fusogenesis. The mega-stable six-helix bundle reported here may represent one of post-fusion states of the fusion core of SARS-CoV S protein.

In addition to the strong hydrophobic interactions, Duquerroy et al. had suggested that the two helices are also stabilized by ion pairs at either end of the HR2 helix: the side chains of Lys929/Glu1163 and Lys903/Glu1188 are within the range of ionic interactions. Such ion pairs can enhance inter-helical stability in α-helical coiled-coils and contribute to the formation of the trimeric structure through minimizing the number of inter-helical electrostatic repulsions and maximizing the number of inter-helical electrostatic attractions [Kohn et al., 1998].

In an attempt to dissect the interaction-determining sequence of HR1, we divided HR1 into two overlapping peptides (HR1-a and HR1-b) and their ability to interact with HR2 and viral-entry attenuation activity were tested. We found that HR1-b (Ile916-Ser950) but not HR1-a (Tyr899-Ala926) interacted with HR2, as demonstrated by CD and LS. Interestingly, peptide HR1-a has a higher virus-entry inhibition activity than HR1-b. This suggests that the N-terminal segment of HR1 may interact with regions other than HR2 of the S protein in receptor-binding and/or fusogenesis.

Learned from the remarkable inhibitory activity of ADS-J1 against HIV-1, future investigation of the interactions responsible for stabilizing the binding of ADS-J1 to on HR1 at the relatively deep groove region of SARS-CoV S protein could provide valuable insight into the discovery of more effective entry inhibitors against SARS-CoV. Our molecular docking modeling shows that the close contact

between the highly hydrophobic groups of ADS-J1 and the hydrophobic residues in deep pocket may block the hydrophobic interactions between HR2 and the deep groove of HR1. Also ADS-J1 may prevent the peripheral ionic interaction between HR1 and HR2 by interacting with the positively charged side-chain of Lys911. The predicted docking energy between ADS-J1 and HR1-DP further provides information to guide these investigations.

EXPERIMENTAL METHODS

Protein Cloning, Expression, and Purification

The gene sequence of SARS-CoV S protein based on the SARS-CoV CUHK-Su10 strain complete genome sequence (GenBank accession no. AY282752) was used. For His_6-HR1 (residues 899–958), the coding sequence was inserted into *Bam*HI/*Sal*I sites of expression vector pET-28a (Novagen, Darmstadt, Germany). For GST-HR2/GST-removed-HR2 (residues 1,145–1,192), the coding sequence was inserted into EcoRI/*Sal*I sites of expression vector pGEX-6P-1 (GE Healthcare, Fairfield). HR-2-Helix, it was created by linking HR1 (residues 899–958) and HR2 (residues 1,145–1,192) with a ten-amino acid flexible linker (N′-Gly-Gly-Ser-Gly-Glu-Phe-Gly-Gly-Ser-Gly-C′). The coding sequences of HR1 and HR2 were inserted into *Bam*HI/EcoRI and EcoRI/*Sal*I sites of expression vector pGEX-6P-1, respectively.

Protein expression was done using *E. coli* strain BL21 (DE3) pLysS (Novagen). Expression was induced by adding 0.1 mM of IPTG to cultures harboring pET-28a-His_6-HR1, pGEX-6P-1-GST-HR2 and pGEX-6P-1-HR-2-Helix plasmids, respectively, when absorption at 600 nm of the culture reached 0.6 AU. The cells were harvested by centrifugation at 3,200*g* at 4°C after 6 h of induction. The cell pellets were resuspended in the PBS and sonicated. The suspension was centrifuged at 48,000*g* for 45 min at 4°C. For His_6-HR1, the supernatant was loaded onto a column of His-Select Nickel Affinity resin (Sigma-Aldrich-Fluka, St. Louis, MO). After washing the column with 10 bed volumes of PBS containing 50 mM imidazole, the His-tagged His_6-HR1 protein was eluted using PBS containing 300 mM imidazole. For GST-HR2 and GST-HR-2-Helix, the supernatant of the bacterial lysate was loaded onto a column of Glutathione Sepharose™ 4 Fast Flow affinity resin (GE Healthcare). After washing the column with 10 bed volumes of PBS, the GST-tagged proteins were eluted using PBS containing 10 mM reduced glutathione and then subjected to size-exclusion chromatography (SEC) over a HiLoad™ 16/60 Superdex™ 75 Prep Grade column (GE Healthcare). GST-removed-HR2 and HR-2-Helix were generated by on-column cleavage of the GST-tagged GST-HR2 and GST-HR-2-Helix using PreScission Protease (GE Healthcare). The GST-removed-HR2 and HR-2-Helix proteins were eluted using PBS.

The eluted His_6-HR1, GST-removed HR2 and HR-2-Helix were concentrated and further purified by preparative reverse-phase high-performance liquid chromatography (RP-HPLC) column (Alltima C18 5 μm, 250 mm × 10 mm, Alltech, Kentucky) on an Agilent Technologies 1100 Series HPLC system. A linear gradient 2% acetonitrile/min over water (containing 0.05% trifluoroacetic acid) was used. Fractions of RP-HPLC containing target proteins were lyophilized overnight, dissolved in PBS and characterized by analytical RP-HPLC, amino acid analysis, and MALDI-TOF MS on an ABI 4700 MALDI TOF/TOF Analyzer (Applied Biosystems, Foster City, CA).

Peptide Synthesis

Peptides HR1-a, HR1-b and HR2 were synthesized using amide resin with conventional solid-phase 9-fluorenylmethoxycarbonyl (Fmoc) synthesis chemistry as described previously [Chu et al., 2006]. The peptides were purified by reverse phase (RP) HPLC, lyophilized and dissolved in PBS and characterized by analytical RP-HPLC, amino acid analysis, and MALDI-TOF MS on an ABI 4700 MALDI TOF/TOF Analyzer.

Native Polyacrylamide Gel Electrophoresis (PAGE) Analysis

HR1-a and HR1-b were incubated with an equal molar concentration of HR2 respectively at 37°C for 1 h (the final concentrations of HR1-a, HR1-b and HR2 were 50 μM). After incubation, the samples were mixed with 6X native gel-loading buffer (300 mM Tris–HCl (pH 6.8), 0.6% (w/v) bromophenol blue, 60% glycerol) and were then loaded to a 20% Tris–tricine gel in Tris–tricine running buffer. Gel electrophoresis was carried out with 100 V constant

voltages at room temperature for 2 h. The gel was stained with Coomassie blue.

Laser Light Scattering (LS) Analysis

A Superdex^{TM} 75 10/300 GL Columns (GE Healthcare), which was connected in-line with the laser light scattering (LS) system (Wyatt Technology, Santa Barbara, CA) using WyattQELS^{TM} (Quasi-Elastic-Light-Scattering) detector combination with miniDAWN and ptilab® DSP for LS and refractive index (RI), respectively. ÄKTA^{TM}FPLC^{TM} was used for solvent delivery. Prior to sample injection, the column was equilibrated with PBS which was used as a mobile phase at a flow rate of 0.75 ml/min. The whole process was carried out at room temperature. Sample volume of 150-μl was routinely injected. Protein concentrations were 1.25 mg/ml (His_6-HR1 and GST-removed HR2) or 1 mg/ml (HR-2-Helix) For the complex formation between His_6-HR1 and GST-removed HR2, the proteins were incubated in an equal molar concentration at 37°C for 1 h.

Molecular weight of His_6-HR1, GST-removed HR2, the His_6-HR1/GST-removed HR2 complex, HR-2-Helix, HR1-b, HR2 and HR1-b/HR2 complex were determined using ASTRA software (Wyatt Technology) using the light scattering (LS) and refractive index (RI) data acquired across the entire elution volume. A dn/dc value of 0.185 ml/g was used. The molar mass distribution plots were generated.

Circular Dichroism (CD) Analysis

Protein/peptide samples in PBS were incubated at 37°C for 1 h. After incubation, CD spectra were measured on a JASCO J-810 spectropolarimeter equipped with a peltier-type temperature control unit. Wavelength spectra were scanned from 260 to 190 nm at 20 nm min^{-1} at 37°C using a 1 mm path-length cuvette. The thermal stability of the proteins/peptides was measured by recording the molar ellipticity at 222 nm of degassed protein sample at a heating rate of 1°C/min. The cuvette was capped to minimize evaporation. Final concentration of proteins/peptides were 25 μM (His_6-HR1 and GST-removed HR2) or 50 μM (HR-2-Helix, HR1-a, HR1-b and HR2). For the analysis of complex formation, the proteins/peptides were mixed in equal molar concentrations and incubated at 37°C for 1 h before taking measurement.

HIV-luc/SARS Pseudotyped Virus Entry Inhibition Assay

To produce HIV-luc/SARS pseudotyped virus, 10 μg of HIV-1 luciferase reporter vector pNL4.3.Luc.E-R-luc (HIV-luc) and 10 μg of codon-optimized SARS-CoV S protein expression plasmid (pcTSh) were co-transfected into 293 T cells by calcium phosphate coprecipitation. The construction of the plasmids have been described previously [Connor et al., 1995; Nie et al., 2004]. The pseudotyped virus was harvested after 48 h of incubation and purified by ultracentrifugation through a CsCl density gradient at 50,000*g* for 4 h. The supernatant containing the pseudotyped virus was collected, filtered through a 0.45 μm Millipore-sized membrane and stored at −80°C until used. To measure luciferase activity, 20-μl aliquots of the pseudotyped virus were added to 100 μl of Luciferase Assay Reagent (Luciferase Assay Substrate pre-mixed with Luciferase Assay Buffer, Promega, USA). Luciferase activity was measure 10 s using a Wallac Multilabel 1450 Counter (Perkin-Elmer, Singapore).

For peptide inhibitors and small molecule inhibitor assays, the supernatant containing 5 ng of pseudotyped virus was incubated with different concentrations of peptides and small molecules at 37°C for 30 min. The mixture was then transferred into 96-well plates seeded with Vero-E6 cells (8×103 cells/well) in triplicate. After overnight incubation, the medium was replaced, and the sample was incubated for 36 h. The cells were then measured for luciferase activities as described above.

Molecular Docking Analysis of ADS-J1

All 3D molecular modeling studies were performed on an Insight II molecular modeling platform (Accelrys Software, Inc., USA) running on Silicon Graphics Octane2 workstations (Silicon Graphics, Inc., USA). The consistent valence force field (CVFF) was selected in all the simulations. The structure of the anti-HIV-1 agent ADS-J1 was constructed with BUILDER module. In this module, the two-dimensional image of ADS-J1 was constructed using SKETCHER and was automatically converted into a three-dimensional model by CONVERTER. The X-ray crystal structure of the SARS-CoV S protein fusion core (PDB 1WNC) was obtained from the Protein Data Bank (http://www.rcsb.org/pdb/) and used as a

starting model. One of the HR1 helices from the six-helix coiled-coil bundle was extracted to generate the target site for docking of ADS-J1. Hydrogen atoms were added to the HR1 structure using the BUILDER module. Force field potentials and partial charges were then assigned for both of the structures of HR1 and ADS-J1. These structures were energy-minimized separately using the DISCOVER module and used as the pre-docking structures. A distance-dependent dielectric constant of 80.0 (aqueous solvent) and non-bonded distance cutoff of 20 Å were used throughout the energy minimization and molecular dynamics simulation. Initially, the structures of HR1 and ADS-J1 were minimized for 5,000 iterations of steepest descent energy minimization. Molecular dynamics simulations were applied to the resulting structures: the energy-minimized structures were equilibrated at 300 K for 10 picoseconds (ps) and then subjected to 100-ps dynamics simulations at the same temperature with sampling steps of 1 femtosecond (fs). According to information derived from the X-ray crystallographic structure of the fusion core [Supekar et al., 2004; Xu et al., 2004a; Duquerroy et al., 2005], four hydrophobic residues from the HR2 (Leu1168, Val1171, Leu1175, and Leu1179) penetrate into one of the three hydrophobic deep pockets or cavities formed between Phe909 and Leu920 on the deep groove region of HR1 (Fig. 8). Therefore, the region containing all residues (5.0 Å radius) around this deep pocket was selected as the target site (named HR1-DP) and set up as a grid with the DOCKING module. The non-bonded energetics of this region was pre-calculated on the grid. ADS-J1 was first docked into HR1-DP by manual docking using the DOCKING module. The best docking position was based on the docking energy of the ADS-J1/HR1-DP complex. Thousand of orientations of ADS-J1 were searched by maneuvering it in the HR1-DP manually until the energy minimum was found. The resultant complex was subjected to energy minimization and molecular dynamics simulation using the DISCOVER module. An 8.0 Å cutoff for the calculation of non-bonded interactions and the distance-dependent dielectric constant of 80.0 (aqueous solvent) and non-bonded distance cutoff of 20 Å were used throughout the energy minimization and molecular dynamics simulation. Initially, the complex was minimized for 5,000 iterations of steepest descent energy minimization. The resulting structure was then used as a starting point for sampling conformational space using molecular dynamics. The energy-minimized complex was equilibrated at 300 K for 10 ps. Following this, a 100 ps dynamics simulation was carried out at the same temperature, and the structure was sampled at steps of 1 fs. The sampled structure was subsequently energy-minimized using conjugate gradient minimization. Ultimately, the total docking energy between ADS-J1 and HR1-DP in the energy minimized complex was calculated using the DOCKING module. van der Waals and electrostatic energies were included in the docking.

ACKNOWLEDGMENTS

This work was supported by the SARS Special RGC Grant (CUHK4536/03M), the Croucher Foundation and special SARS funding grant from GreaterChina Technology Group Ltd.

REFERENCES

Chim SS, Tsui SK, Chan KC, Au TC, Hung EC, Tong YK, Chiu RW, Ng EK, Chan PK, Chu CM, Sung JJ, Tam JS, Fung KP, Waye MM, Lee CY, Yuen KY, Lo YM. 2003. Genomic characterisation of the severe acute respiratory syndrome coronavirus of Amoy Gardens outbreak in Hong Kong. Lancet 362:1807–1808.

Choy WY, Lin SG, Chan PK, Tam JS, Lo YM, Chu IM, Tsai SN, Zhong MQ, Fung KP, Waye MM, Tsui SK, Ng KO, Shan ZX, Yang M, Wu YL, Lin ZY, Ngai SM. 2004. Synthetic peptide studies on the severe acute respiratory syndrome (SARS) coronavirus spike glycoprotein: Perspective for SARS vaccine development. Clin Chem 50:1036–1042.

Chu LH, Choy WY, Tsai SN, Rao Z, Ngai SM. 2006. Rapid peptide-based screening on the substrate specificity of severe acute respiratory syndrome (SARS) coronavirus 3C-like protease by matrix-assisted laser desorption/ionization time-of-flight mass spectrometry. Protein Sci 15:699–709.

Connor RI, Chen BK, Choe S, Landau NR. 1995. Vpr is required for efficient replication of human immunodeficiency virus type-1 in mononuclear phagocytes. Virology 206:935–944.

Deng Y, Liu J, Zheng Q, Yong W, Lu M. 2006. Structures and polymorphic interactions of two heptad-repeat regions of the SARS virus S2 protein. Structure 14: 889–899.

Duquerroy S, Vigouroux A, Rottier PJ, Rey FA, Bosch BJ. 2005. Central ions and lateral asparagine/glutamine zippers stabilize the post-fusion hairpin conformation of the SARS coronavirus spike glycoprotein. Virology 335: 276–285.

Eckert DM, Kim PS. 2001a. Design of potent inhibitors of HIV-1 entry from the gp41 N-peptide region. Proc Natl Acad Sci USA 98:11187–11192.

Eckert DM, Kim PS. 2001b. Mechanisms of viral membrane fusion and its inhibition. Annu Rev Biochem 70:777–810.

Hofmann H, Pohlmann S. 2004. Cellular entry of the SARS coronavirus. Trends Microbiol 12:466–472.

Kilby JM, Hopkins S, Venetta TM, DiMassimo B, Cloud GA, Lee JY, Alldredge L, Hunter E, Lambert D, Bolognesi D, Matthews T, Johnson MR, Nowak MA, Shaw GM, Saag MS. 1998. Potent suppression of HIV-1 replication in humans by T-20, a peptide inhibitor of gp41-mediated virus entry. Nat Med 4:1302–1307.

Kohn WD, Kay CM, Hodges RS. 1998. Orientation, positional, additivity, and oligomerization-state effects of interhelical ion pairs in alpha-helical coiled-coils. J Mol Biol 283:993–1012.

Ksiazek TG, Erdman D, Goldsmith CS, Zaki SR, Peret T, Emery S, Tong S, Urbani C, Comer JA, Lim W, Rollin PE, Dowell SF, Ling AE, Humphrey CD, Shieh WJ, Guarner J, Paddock CD, Rota P, Fields B, DeRisi J, Yang JY, Cox N, Hughes JM, LeDuc JW, Bellini WJ, Anderson LJ. 2003. A novel coronavirus associated with severe acute respiratory syndrome. N Engl J Med 348:1953–1966.

Lee N, Hui D, Wu A, Chan P, Cameron P, Joynt GM, Ahuja A, Yung MY, Leung CB, To KF, Lui SF, Szeto CC, Chung S, Sung JJ. 2003. A major outbreak of severe acute respiratory syndrome in Hong Kong. N Engl J Med 348: 1986–1994.

Lio P, Goldman N. 2004. Phylogenomics and bioinformatics of SARS-CoV. Trends Microbiol 12:106–111.

Liu S, Xiao G, Chen Y, He Y, Niu J, Escalante CR, Xiong H, Farmar J, Debnath AK, Tien P, Jiang S. 2004. Interaction between heptad repeat 1 and 2 regions in spike protein of SARS-associated coronavirus: Implications for virus fusogenic mechanism and identification of fusion inhibitors. Lancet 363:938–947.

Nie Y, Wang P, Shi X, Wang G, Chen J, Zheng A, Wang W, Wang Z, Qu X, Luo M, Tan L, Song X, Yin X, Chen J, Ding M, Deng H. 2004. Highly infectious SARS-CoV pseudotyped virus reveals the cell tropism and its correlation with receptor expression. Biochem Biophys Res Commun 321:994–1000.

Spiga O, Bernini A, Ciutti A, Chiellini S, Menciassi N, Finetti F, Causarono V, Anselmi F, Prischi F, Niccolai N. 2003. Molecular modelling of S1 and S2 subunits of SARS coronavirus spike glycoprotein. Biochem Biophys Res Commun 310:78–83.

Supekar VM, Bruckmann C, Ingallinella P, Bianchi E, Pessi A, Carfi A. 2004. Structure of a proteolytically resistant core from the severe acute respiratory syndrome coronavirus S2 fusion protein. Proc Natl Acad Sci USA 101:17958–17963.

Tripet B, Howard MW, Jobling M, Holmes RK, Holmes KV, Hodges RS. 2004. Structural characterization of the SARS-coronavirus spike S fusion protein core. J Biol Chem 279:20836–20849.

Wolf E, Kim PS, Berger B. 1997. MultiCoil: A program for predicting two- and three-stranded coiled coils. Protein Sci 6:1179–1189.

Xu Y, Lou Z, Liu Y, Pang H, Tien P, Gao GF, Rao Z. 2004a. Crystal structure of severe acute respiratory syndrome coronavirus spike protein fusion core. J Biol Chem 279: 49414–49419.

Xu Y, Zhu J, Liu Y, Lou Z, Yuan F, Liu Y, Cole DK, Ni L, Su N, Qin L, Li X, Bai Z, Bell JI, Pang H, Tien P, Gao GF, Rao Z. 2004b. Characterization of the heptad repeat regions, HR1 and HR2, and design of a fusion core structure model of the spike protein from severe acute respiratory syndrome (SARS) coronavirus. Biochemistry 43:14064–14071.

Zhu J, Xiao G, Xu Y, Yuan F, Zheng C, Liu Y, Yan H, Cole DK, Bell JI, Rao Z, Tien P, Gao GF. 2004. Following the rule: Formation of the 6-helix bundle of the fusion core from severe acute respiratory syndrome coronavirus spike protein and identification of potent peptide inhibitors. Biochem Biophys Res Commun 319:283–288.